Molecular Crystals and Liquid Crystals
Publication details, including instructions for authors and subscription information:
http://www.tandfonline.com/loi/gmcl20

Structural and Optical Properties of Al-Zn-Cu Thin Films Prepared by DC-Magnetron Sputtering at Different Sputtering Powers

Laya Dejam [a] & S. Mohammad Elahi [a]
[a] Plasma Research Center , Science and Research Branch Islamic Azad University , Tehran , Iran
Published online: 09 Jul 2013.

To cite this article: Laya Dejam & S. Mohammad Elahi (2013) Structural and Optical Properties of Al-Zn-Cu Thin Films Prepared by DC-Magnetron Sputtering at Different Sputtering Powers, Molecular Crystals and Liquid Crystals, 577:1, 59-70, DOI: 10.1080/15421406.2013.786644

To link to this article: http://dx.doi.org/10.1080/15421406.2013.786644

Mol. Cryst. Liq. Cryst., Vol. 577: pp. 59–70, 2013

ISSN: 1542-1406 print/1563-5287 online
DOI: 10.1080/15421406.2013.786644

Taylor & Francis
Taylor & Francis Group

Structural and Optical Properties of Al–Zn–Cu Thin Films Prepared by DC-Magnetron Sputtering at Different Sputtering Powers

LAYA DEJAM AND S. MOHAMMAD ELAHI*

Plasma Research Center, Science and Research Branch Islamic Azad University, Tehran, Iran

Al–Zn–Cu thin films were deposited using DC-magnetron sputtering on glass substrates at room temperature in pure Ar gas environment. The influence of variation power sputtering from 30–120 W on the structural and optical properties has been studied. The X-ray diffraction (XRD) patterns show amorphous structure for all films. The atomic force microscopy (AFM) images revealed a homogeneous Al–Zn–Cu dispersion within the layer in low power sputtering. The optical transmittance spectra showed that the optical transmittance in the visible was decreased with increased power sputtering. By increasing thickness of films, optical band gap in films decreased, and intensity of PL is increased.

Keyword Al-Zn-Cu thin film; optical band gap; particle size; photoluminescence

Introduction

Shape memory alloys (SMAs) have been implemented in a number of high performance applications requiring high work densities, large recoverable deformations, and high stresses. More recently, SMAs have become excellent candidates for microactuators when fabricated as thin films. Their work output density ($\sim$50 MJm^{-3}) exceeds that of other microactuator mechanisms and they can yield large strokes ($\sim$5%) and forces ($\sim$30 mN). Moreover, thin film SMAs heat on the order of milliseconds by low voltage ($\sim$5 V) Joule heating, and, unlike bulk SMAs (wires, beams, etc.), their small mass and large surface-to-volume ratio allow fast cooling, potentially permitting switching frequencies on the order of 100 Hz [1].

Current microscale SMA applications include microgrippers [2], micropumps, and microcantilever switches [3,4]. Most of these applications rely on the one-way memory effect and require a biasing mechanism for full actuation. However, microdevices using functionally graded films can achieve two-way, out-of-plane displacement with a smaller footprint than conventional micromechanisms [5,6].

In conjunction with advancing fabrication and film characterization technologies, initial thin film SMA models have been developed [7–10]. Established bulk models may be considered for thin film SMAs, provided modifications are made to address issues of scale and the microfabrication process [11].

*Address correspondence to S. Mohammad Elahi, Plasma Research Center, Science and Research Branch Islamic Azad University, Tehran, Iran. E-mail: Smohammad_elahi@yahoo.com

The SMAs such as Cu-based binary and ternary (Cu–Zn, Cu–Al, Cu–Zn–Al, and Cu–Al–Ni) and Ni–Ti are usually used as functional actuators and sensors [12]. Cu–Zn–Al alloys exhibit, in a certain range of composition, the Shape Memory Effect (SME), that is, when a material have the capacity to recover their shape with a simple heating after suffer an apparent plastic deformation. SME is due to martensitic-austenitic phase transformation depending on the temperature. The lattice structure changes in Cu–Zn–Al alloys associated with the martensitic transformation are from the crystal structure DO_3 or $L2_1$ at higher temperature (austenitic phase) to 18R (martensitic phase) at lower temperature. Along with this phase transformation occurs significant changes in mechanical, physical, chemical, electrical, and optical properties, including yield stress, elastic modulus, damping, hardness, electrical resistivity, thermal conductivity, thermal expansion, and surface roughness [13].

The influence of the grain size in the properties of SMA has been observed in different systems, especially the dependence of the martensitic transformation behavior in nanostructure SMA. It has been reported that the transformation takes place in bulk materials after a severe deformation and different heat treatments when the grain size of the alloy is around 40 nm [14–19]. The development of SMA with controlled grain size is interesting for applications. It must be pointed out that, in bulk materials with nanograins, SME could be limited by grain size [19]. It was suggested that grain boundaries hinder the transformation. However, grain boundaries should not be a limitation in nanoparticles, so it can be expected that the transformation will take place [13].

On the other hand, several potential applications of ZnO for novel optical devices as, for instance blue light emitters, lasers devices, or UV sensors [20] were proposed. In addition, ZnO doped with transition metal (TM = Co, Cu, Mn, ...) ions is intensively studied for spintronics applications [21,22]

Al doped ZnO thin films have a significant optical transmission in the visible which makes them highly sought in the photovoltaic industry [20]. In recent years, the zinc oxide thin films deposition with acceptable quality has been achieved by several techniques such as chemical vapor deposition [21], laser ablation deposition [23], RF magnetron sputtering [24]. ... etc., ZnO can be used in components of micro-and opto-electronics such as field effect transistors [25], photodiodes [26], light emitting diodes [27], and laser diodes [28]. This material, with an important binding energy of excitons (60 meV), has the property to interact strongly with light and, therefore, it has become a potential candidate for the realization of a new very low threshold class of lasers. It is also characterized by a large transmittance coefficient that exceeds 90% in the visible. Because of its wide gap (3.37 eV), ZnO can be doped or codoped to improve its optical properties. Among the doping elements, aluminum can be a good candidate to excite the photoluminescence (PL) in the UV-visible spectral range. This is due to its new nonlinear optical properties, the room temperature excitonic emission and the quantum confinement effect [29].

In our knowledge, there is no report on the properties of Aluminum zinc copper thin films. In this work, we use an Al–Zn–Cu target for sputtering that it prepared just with press of metals powders and we report detailed study of influences thickness and power sputtering on structural and optical properties of Al and Cu doped ZnO thin films.

Experimental

Al–Zn–Cu films were deposited by Direct Current planer-magnetron sputtering. Target was a disk (10 cm diameter and 5 mm thickness) with 55% Al, 40% Zn, and 5% Cu that prepared from powders of Al, Zn, and Cu metals. The purity of metals powder used in this study

Table 1. Sputtering power, film thickness, and band gap of samples

Sample	1	2	3	4
Power of sputtering (W)	30	37.5	60	120
Film thickness (nm) (standard error ±5 nm)	28	68	123	406
Band gap (eV)	3.65	3.58	3.5	—

was 99.99%. The sputtering chamber was evacuated to less than 3×10^{-5} mbarr pressures with rotary and diffusion pumps combination, and then argon gas (Purity 99.999%) was introduced to the chamber as a sputtering gas. Glass substrate 10 mm × 20 mm square were distanced 45 mm from target. Before deposition, substrates were cleaned by ultrasonic waves in acetone and alcohol. Sputtering time and working gas pressure were fixed at 30 s and 1×10^{-2} mbar, respectively. Sputtering power was changed from 30 to 120 W that presented in Table 1. In the deposition process, no external heating was provided. After film deposition, X-ray diffraction (XRD) was performed on STOE-XRD diffractometer using Cu-K_α line ($l = 0.15406$ nm). Energy Dispersive X-Ray (EDX) was measured on Philips XL Series 30. Atomic Force Microscopy (AFM) micrographs were taken using Auto probe CP from Park Scientific Instrument. The optical properties of thin films were examined at room temperature by a UV–Vis absorption spectrophotometer (PG Instruments Ltd). Room temperature PL of the samples was measured to characterize the luminescence properties of films, using a Cary Eclipse spectrometer equipped with a xenon lamp. A DEKTAK3 profilmeter was employed to measure the thickness of the growth films.

Results and Discussion

Growth Rate and Film Composition

Growth rate was determined by dividing the film thickness by the sputtering time. This deposition parameter is important in film thickness control, especially for precise multilayer preparation [30]. Fig. 1 shows the growth rate as a function of power sputtering. Growth rate increases linearly with the sputtering power. We attribute this dependence relationship to the determinacy of sputter growth rate on the Ar ion flux (J_{ion}) and its average kinetic energy (KE_{av}) upon striking the target.

These are a function of dc applied voltage (V_{dc}), according to Langmuir–Child relationship [31] and average kinetic energy equation in dc glow discharge [32]:

$$J_{\text{ion}} \propto V_{\text{dc}}^{3/2} \tag{1}$$

$$\text{KE}_{\text{av}} \propto V_{\text{dc}}. \tag{2}$$

The high Ar ion flux generally results in substantial ion bombardment on the target while the high kinetic energy of these ions increases the probability that the impacts of incident ions will eject target atoms. These two mechanisms are proportional to dc applied voltage and sputtering power, and hence contribute to the increase of the growth rate [33].

The chemical composition of Al–Zn–Cu films was analyzed by an EDX spectroscopy. Fig. 2 shows the typical EDX spectrum corresponding to the Al–Zn–Cu film prepared with power sputtering of 120 W.

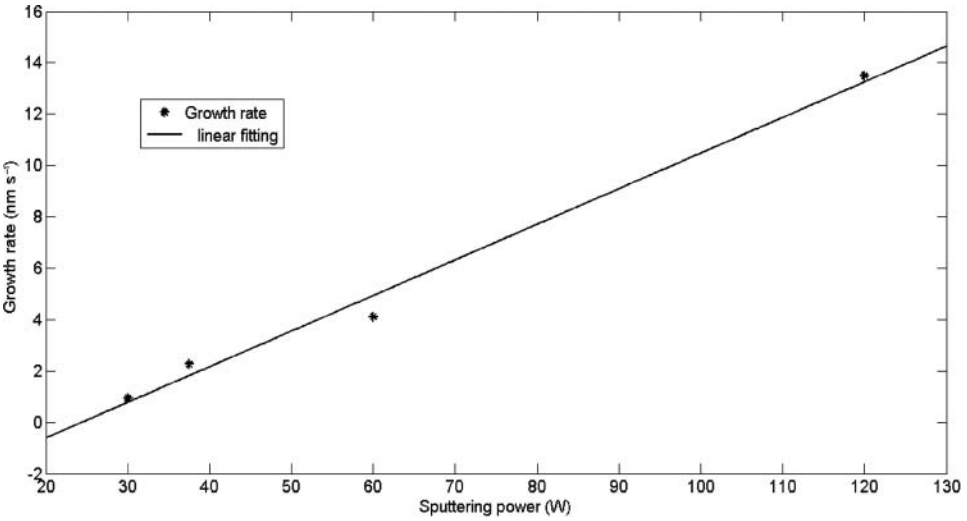

Figure 1. Growth rate of Al–Zn–Cu films on glass substrate.

The amount of atoms arriving at the substrate surface is observed to be inversely proportional to the Al and Zn content in the target. It means that, the amount of Al in film is more than Zn. This decreasing arriving possibility could be explained by the decreasing sputtered atoms, since sputtering yield of Al is lower than sputtering yield of Zn.

XRD Analysis

The crystal structure of Zn–Al–Cu films were investigated by XRD. Fig. 3(a) shows the patterns of target. All the peaks belong to Zn, Al, Cu, and ZnO.

Figure 3(b) shows the XRD patterns of the as-sputtered thin films at various powers sputtering. All the films had approximately amorphous structure. It can be explain that the time of sputtering was not enough for crystallization of films or it might be the rate of sputtering was very fast that atoms in films did not have time for crystallization. And or some other parameters, like substrate temperature, are important.

AFM Illustration

Surface morphology of Al–Zn–Cu films was examined by the AFM, as shown in Fig. 4. The 1×1 μm^2 3D AFM micrographs show the features of structural change and grain growth for Al–Zn–Cu films deposited at 30–120 W on glass substrate at room temperature. It was observed that the AFM micrograph of the Al–Zn–Cu films deposited at 30 and 37.5 W (Figs. 4(a)–(b)) exhibits uniform surface, indicating its amorphous-like behavior. Figs. 4(c)–(d) show the AFM micrographs for Al–Zn–Cu films deposited at 60 and 120 W, respectively. In these micrographs, particle size protruding from the film surface develops in the Al–Zn–Cu films and is enhanced with increasing sputtering power. In Figs. 4(a)–(b), the grains are smaller and densely packed producing smoother surface in micrograph of Figs. 4(c)–(d). In Figs. 4(c)–(d), the grains were observed to have agglomerated together and formed smaller number of bigger grains with voided boundaries and the nanoparticle grains are not homogeneously distributed all over the substrate surfaces. Comparing the

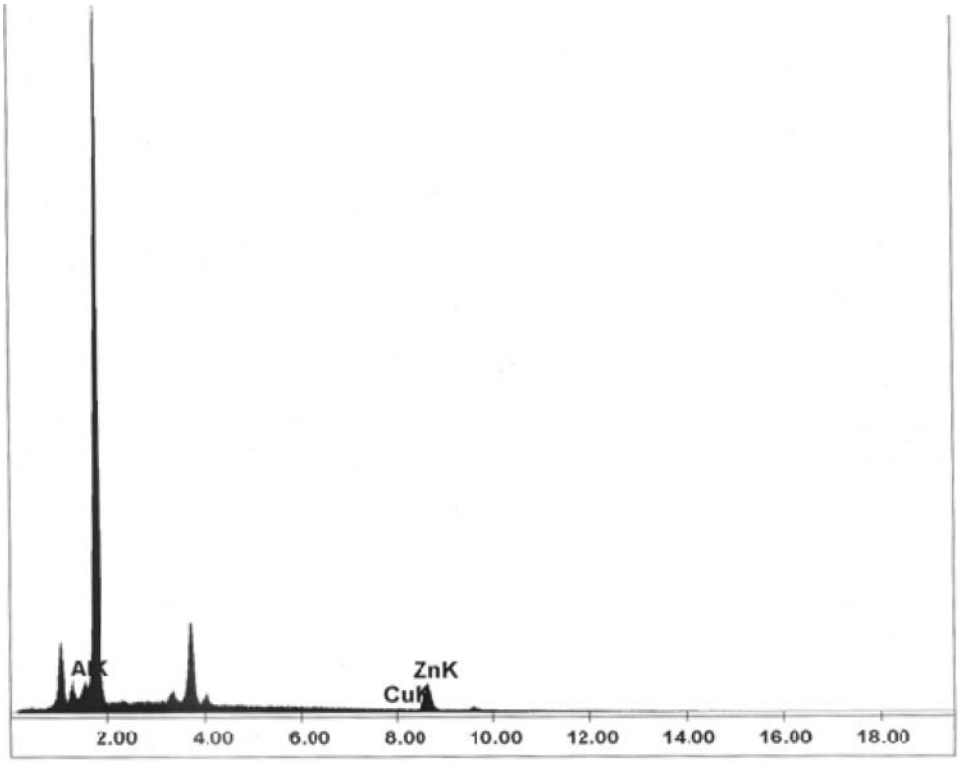

EDAX ZAF Quantification (Standardless)
Element Normalized

Element	Wt %	At %
AlK	20.50	38.14
CuK	2.26	1.30
ZnK	77.43	60.05
Total	100.00	100.00

Element	Net Inte.	Bkgd Inte.	Inte. Error	P/B
AlK	44.57	16.63	2.27	2.68
CuK	2.60	9.73	17.44	0.27
ZnK	72.30	8.54	1.60	8.54

Figure 2. EDX spectrum of Al–Zn–Cu thin films.

micrographs in Fig. 4, Al–Zn–Cu films deposited at higher sputtering power (Fig. 4(d)) exhibits big particle size and more voided boundaries. We have known that the higher sputtering power giving better microstructure is due to the fact that sputtering power helps to increase the surface mobility [34, 35], which is required to form continuous film [31]. The increase in the particle size as a result of bombardment to the growth surface by more energetic particles with increasing sputtering power has been reported by Song et al. [36]. The highly energized inert Ar ions could provide translational kinetic energy to the adatoms.

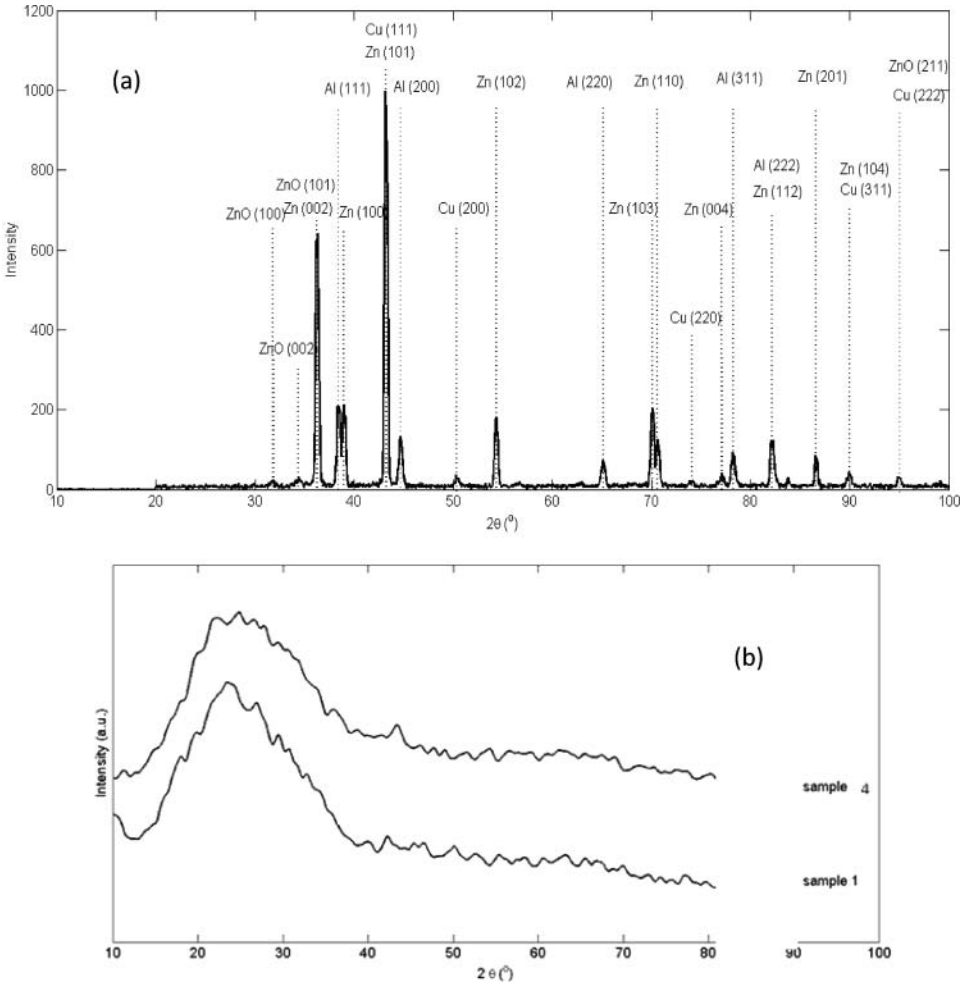

Figure 3. (a) XRD pattern of Al–Zn–Cu target. (b) Al–Zn–Cu thin films.

The surface diffusion of these adatoms was then enhanced with the momentum transfer to the growing surface. Where adatoms diffusion length becomes larger than distance between cluster sites, voided boundaries become filled by diffusing adatoms, and the film develops the characteristics void-free structure. But in this work time of sputtering was just 30 s so one could conclude that with increasing of sputtering power surface diffusion cause to have larger particle but the adatoms diffusion length becomes less than distance between cluster sites so voided boundaries do not become filled by diffusing adatoms.

Optical Properties

The optical transmission was measured by a UV-Vis spectrometer. Fig. 5 gives the spectra for all the Al–Zn–Cu films. Transmittance of Al–Zn–Cu films increases with decreasing the film thickness, which is a natural result of absorption law for thin film semiconductors. Fig. 6 shows absorption coefficient of Al–Zn–Cu thin films as one can notice the fundamental absorption edge of the films shift to higher wavelengths as the film thickness is reduced. The

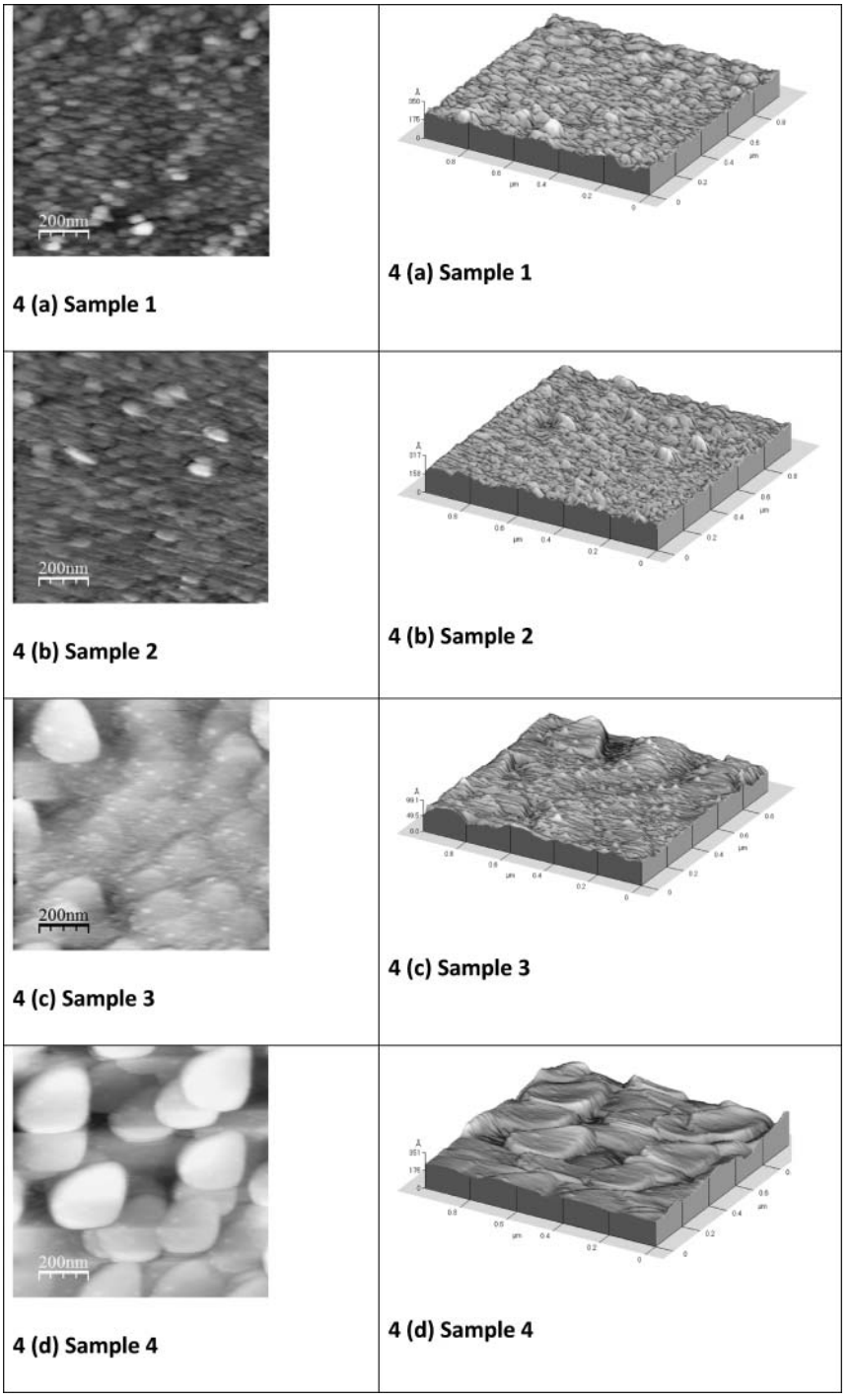

Figure 4. AFM image of Al–Zn–Cu thin films on glass.

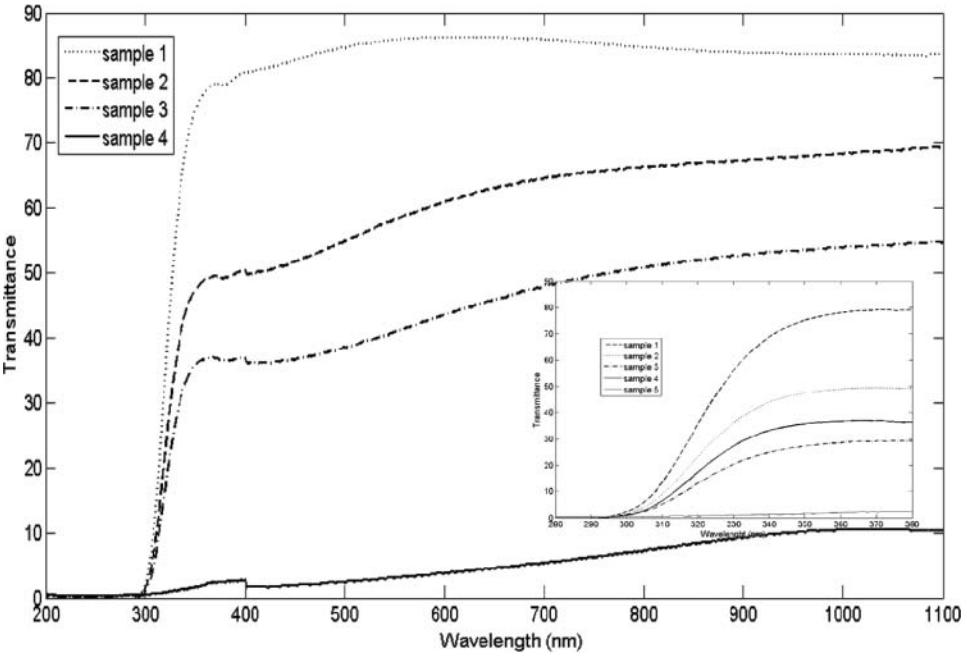

Figure 5. Transmittance spectra of Al–Zn–Cu thin films on glass substrate.

optical band gap E_g of the films was estimated by extrapolating linear portions of $(\alpha h\nu)^{1/2}$ against photon energy $(h\nu)$, where α is the absorption coefficient. With the knowledge of thickness of the film d and transmittance T, α was calculated using the expression $\alpha = (1/d)\ln(1/T)$. The measured band gap as a function of sputtering power is shown to Fig. 7

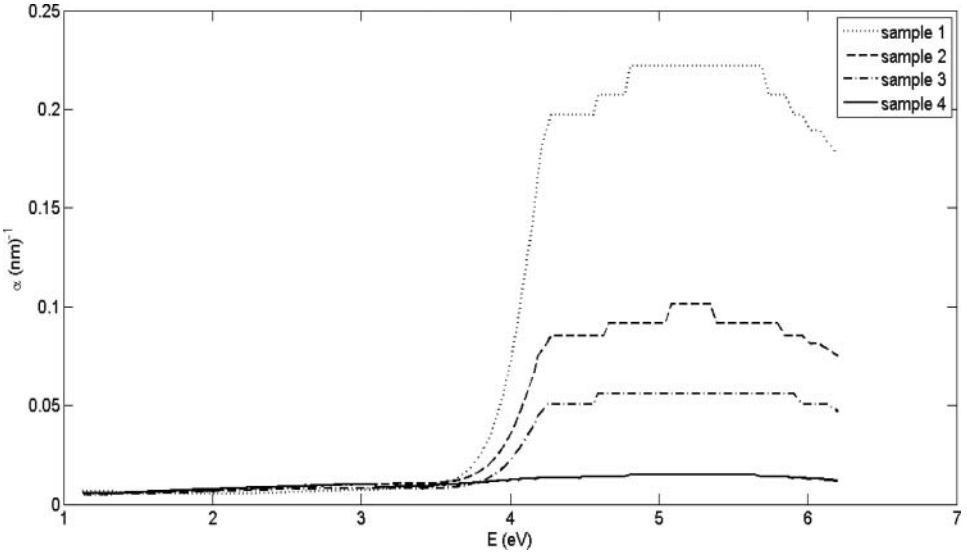

Figure 6. Absorption coefficient of Al–Zn–Cu thin films on glass substrate.

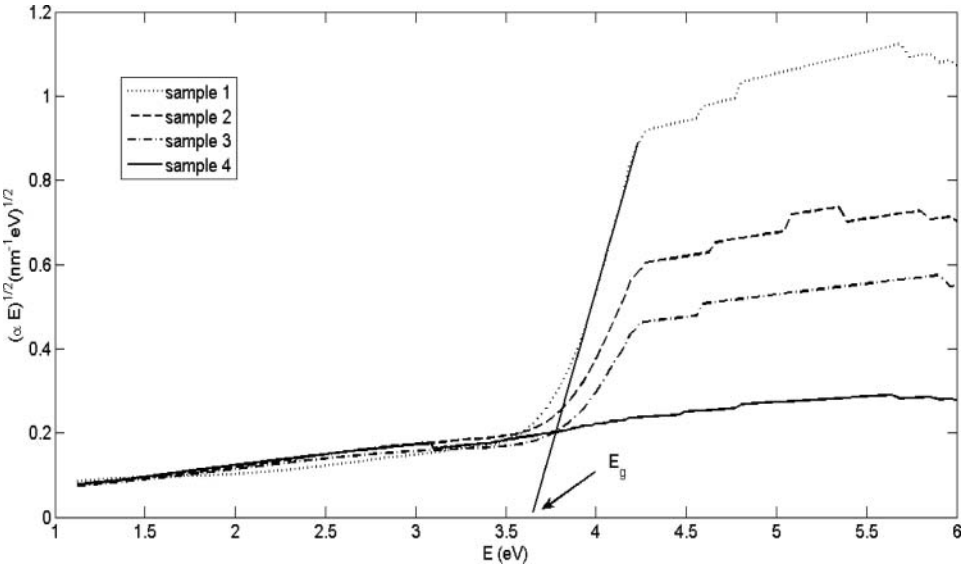

Figure 7. Plot of $(\alpha E)^{1/2}$ vs. photon energy for Al–Zn–Cu thin films.

and the magnitude of band gap illustrated in Table 1. By increasing the thickness of films of the absorption edge is shifted to higher wavelength (red shift) while for thick films (greater than 400 nm) there was no absorption edge. These results are consistence with the result of AFM measurement, in which the particle size was on increasing function of the film thickness. On the other hand, by increasing film thickness the optical band gap of them decreased.

The room temperature PL spectra of as prepared Al–Zn–Cu films are shown in Fig. 8 after excitation at 320 nm. The PL spectra were fitted with Gaussian line shape peaks.

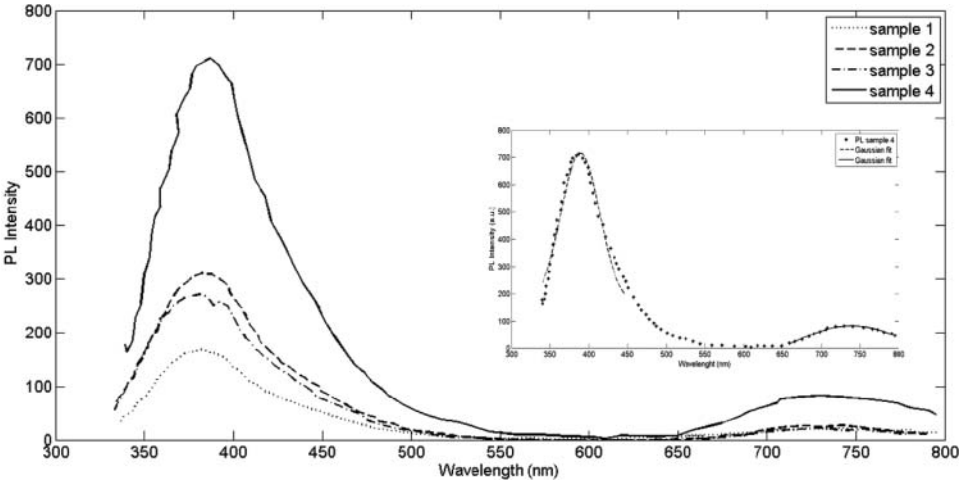

Figure 8. PL spectra of Al–Zn–Cu thin films on glass substrate in room temperature. The inset shows PL spectrum of sample 5 with Gaussian fits.

Table 2. Information of peaks photoluminescence spectra

Sample	Peak positions (nm)	FWHM (nm)	Intensity
1	383.66	44.31	123.5
	739.51	98.56	18.16
2	384.99	48	237.7
	734.89	82.75	30.05
3	385.54	50.55	212.57
	733	76.51	22.01
4	389.86	56.12	594.22
	739.45	144.84	145.88

The obtained peak positions and full-width at half-maximum (FWHM) of the curves are given in Table 2. The influence of power sputtering and film thickness on the intensity and FWHM of emission peaks was investigated. Two emission peaks are observed at 380 nm and 730 nm. We guess the first one corresponds to the band-edge emission as it is reported by [37, 38]. The second one could be related the defects in the thin films [39]. It is seen that the intensity increases with the increase of power sputtering and thickness of films. By increasing thickness of films and power sputtering FWHM of emission peaks increase which is due to the higher number of copper atoms in the more thickened films [40], which causes an increase of emission and reduction of band gap and there would no band gap in the thickest films. The increased intensity of PL is related to the presence of copper atoms in the thin films. The addition of more aluminum atoms leads to the increase of peak intensity and FWHM around 380 nm (as shown in Fig. 8). This behavior could be related the increase of particle size and inhomogeneous by increasing sputtering power. With increasing power sputtering and subsequent increasing of thickness, the particle size is increased and the distribution of particles is more inhomogeneous. On the other hand, the position of this peak is shifted to higher wavelength as the power sputtering is increased.

Conclusion

Al–Zn–Cu films were prepared by 55% Al, 40% Zn, and 5% Cu target with DC magnetron sputtering at various powers sputtering from 30 to 120 W. Growth rate increases linearly with the sputtering power and by increasing power sputtering the thickness of films increased. XRD pattern of films showed all of them were amorphous and EDX of films confirmed that there were Al, Zn, and Cu in films. AFM images showed the particle sizes in thinner films are smaller and densely packed and in thicker films the grains were observed to have agglomerated together and formed smaller number of bigger particles with voided boundaries and the particles are not homogeneously distributed all over the substrate surfaces that it indicated with PL spectra. By increasing thickness of films and power sputtering FWHM of emission peaks are increased subsequently the optical band gap of Al–Zn–Cu films is decreased.

References

[1] Favelukis, J. E., Lavine, A. S., & Carman, G. P. (1999). *Proc. SPIE*, *3668*, 617.
[2] Kohl, M., Krevet, B., & Just, E. (2002). *Sensors Actuat. A Phys.*, *97–98*, 646.

[3] Ishida, A., Sato, M., Yoshikawa, W., & Tabata, O. (2002). *Mater. Sci. Forum*, *394–395*, 487.
[4] Mori, K., Li, H., Roytburd, A. L., & Wuttig, M. (2002). *Jap. Mater. Trans.*, *43*, 951.
[5] Gill, J., Chang, D., Momoda, L., & Carman, G. (2001). *Sensors and Actuators A*, *93*, 148–156.
[6] Gill, J., Ho, K., & Carman, G. P. (2002). *J. Microelectromec. Syst.*, *11*, 68.
[7] Bhattacharyaa, K., & James, R. D. (1999). *J. Mech. Phys. Solids*, *47*, 531.
[8] Gabry, B., Lexcellent, C., et al. (2000). *Thin Solid Films*, *372*, 118.
[9] Jin, Y. M., & Weng, G. J. (2000). *Thin Solid Films*, *376*(1–2), 198–207.
[10] Lexcellent, C., Moyne, S., et al. (1998). *Thin Solid Films*, *324*, 184.
[11] Peirs, J., Reynaerts, D., & Van-Brussel, H. (1998). *Proc. 1998 IEEE Int. Conf. Robot. Autom.*, *2*, 1516.
[12] Izadinia, M., & Dehghani, K. (2011). *Trans. Nonferrous Met. Soc. China*, *21*, 2037.
[13] López Pavón, L. A., Cuellar, E. L., Ballesteros, C., Castro, A. T., Martínez de la Cruz, A., & José de Araújo, C. (2012). *Mater. Res. 15*(3), 341–346.
[14] Fu, Y. Q., Luo, J. K., Flewitt, A. J., Huang, W. M., Zhang, S., Du, H. J., & Milne, W. I. (2009). *International Journal of Computational Materials Science and Surface Engineering (IJCMSSE), 2*, 208.
[15] Fu, Y. Q., Du, H., Huang, W., Zhang, S., & Hu, M. (2004). *Sensors Actuat. A Phys.*, *112*, 395.
[16] Winzek, B., Schmitz, S., Rumpf, H., Sterzl, T., Hassdorf, R., Thienhaus, S., Feydt, J., Moske, M., & Quandt, E. (2004). *Mater. Sci. Eng. A, 378*, 40–46.
[17] Vishoni, R., & Kaur, D. (2010). *Surf. Coat. Technol.*, *204*, 3773.
[18] Filonov, M. R., Brailovski, V., Prokoshkin, S. D., Zhukova, Y. S., & Dubinsky, S. M. (2011). *J. Phys.: Conf. Ser. 291*, 012033.
[19] Zehetbauer, M., Grössinger, R., Krenn, H., Krystian, M., Pippan, R., Rogl, P., Waitz, T., & Würschum, R. (2010). *Adv. Eng. Mat., 12*, 692–700.
[20] Krunks, M., Katerski, A., Dedova, T., Oja Acik, I., & Mere, A. (2008). *Sol. Energ. Mater. Sol. C*, *92*, 1016.
[21] Barnes, T. M., Olson, K., & Woldena, C. A. (2005). *Appl. Phys. Lett.*, *86*, 112112.
[22] Djouadi, D., Chelouche, A., & Aksas, A. (2012). *J. Mater. Environ. Sci.*, *3*(3), 585.
[23] Kim, H., Piqué, A., Horwitz, J. S., Murata, H., Kafafi, Z. H., Gilmore, C. M., & Chrisey, D. B. (2000). *Thin Solid Films V.*, *377*, 798.
[24] Ratheesh Kumar, P. M., Sudha Kartha, C., Vijayakumar, K. P., Abe, T., Kashiwaba, Y., Singh, F., & Avasthi, D. K. (2005). *Semicond. Sci. Technol.*, *20*, 120.
[25] Xu, Z. X., Roy, V. A. L., Stallinga, P., Muccini, M., Toffanin, S., Xiang, H. F., & Che, C. M. (2007). *Appl. Phys. Lett.*, *90*, 223509.
[26] Sun, F., Shan, C. X., Li, B. H., Zhang, Z. Z., Shen, D. Z., Zhang, Z. Y., & Fan, D. (2011). *Opt. Lett.*, *36*, 499.
[27] Ryu, Y. R., Lee, T. S., Lubguban, J. A., White, H. W., Park, Y. S., & Youn, C. J. (2005). *Appl. Phys. Lett.*, *87*, 153504.
[28] Chu, S., Olmedo, M., Yang, Z., Kong, J., & Liu, J. (2008). *Appl. Phys. Lett.*, *93*, 181106.
[29] Wong, E. M., & Searson, P. C. (1999). *Appl. Phys. Lett.*, *74*, 2939.
[30] Lu, J. G., Ye, Z. Z., Zeng, Y. J., Zhu, L. P., Wang, L., Yuan, J., Zhao, B. H., & Liang, Q. L. (2006). *J. Appl. Phys.*, *100*, 073714.
[31] (a) Campbell, S. A. (2001). *The Science and Engineering of Microelectronic Fabrication*, 2nd ed., Oxford University Press: New York, USA, p. 308. (b) Campbell, S. A. (2001). *The Science and Engineering of Microelectronic Fabrication*, 2nd ed., Oxford University Press: New York, USA, p. 312.
[32] Mahan, J. E. (2000). *Physical Vapor Deposition of Thin Films*, Wiley Interscience: New York, p. 178.
[33] Kah-Yoong Chan, & Bee-San Teo (2006). *Microelectr. J.*, *37*, 1064.
[34] Andujar, J. L., Pino, F. J., Polo, M. C., Pinyol, A., Corbella, C., & Bertran, E. (2002). *Diamond Relat. Mater.*, *11*, 1008.
[35] (a) Hwang, D. K., Bang, K. H., Jeong, M. C., & Myoung, J. M. (2003). *J. Cryst. Growth*, *254*, 451 (b) Hwang, D. K., Bang, K. H., Jeong, M. C., & Myoung, J. M. (2003). *J. Cryst. Growth*, *254*, 452.

[36] (a) Song, Y. S., Park, J. K., Kim, T. W., & Chung, C. W. (2004). *Thin Solid Films*, *467*, 118 (b) Song, Y. S., Park, J. K., Kim, T. W., & Chung, C. W. (2004). *Thin Solid Films*, *467*, 120.
[37] Studenikin, S. A., Cocivera, M., Kellner, W., & Pascher, H. (2000). *J. Lumin., 91*, 223–232.
[38] Fonoberov, V. A., Alim, K. A., Balandin, A. A., Faxian Xiu, & Jianlin Liu (2006). *Phys. Rev. B*, *73*, 165317.
[39] Aimable, A., Strachowski, T., Wolska, E., Lojkowski, W., & Bowen, P. (2010). *Processing and Application of Ceramics, 4*, 107–114.
[40] Yanwu Zhu, Chorng-Haur Sow, Ting Yu, Qing Zhao, Pinghui Li, Zexiang Shen, Dapeng Yu, & John Thiam-Leong Thong (2006). *Adv. Funct. Mater., 16*, 2415–2422.